Ferumoxytol nanoparticle uptake in brain during acute neuroinflammation is cell-specific

Heather L. McConnell, B.S.[a], **Daniel L. Schwartz, B.A.**[b], **Brian E. Richardson, Ph.D.**[c], **Randall L. Woltjer, M.D., Ph.D.**[d], **Leslie L. Muldoon, Ph.D.**[a], and **Edward A. Neuwelt, M.D.**[a,e,f]

[a]Department of Neurology, Oregon Health & Science University, Portland, OR, USA

[b]Advanced Imaging Research Center, Oregon Health & Science University, Portland, OR, USA

[c]Department of Molecular and Medical Genetics, Oregon Health & Science University, Portland, OR, USA

[d]Department of Pathology, Oregon Health & Science University, Portland, OR, USA

[e]Department of Neurosurgery, Oregon Health & Science University, Portland, OR, USA

[f]Department of Veterans Affairs, Portland Veterans Affairs Medical Center, Portland, OR, USA

Abstract

Ferumoxytol ultrasmall superparamagnetic iron oxide nanoparticles can enhance contrast between neuroinflamed and normal-appearing brain tissue when used as a contrast agent for high-sensitivity magnetic resonance imaging (MRI). Here we used an anti-dextran antibody (Dx1) that binds the nanoparticle's carboxymethyldextran coating to differentiate ferumoxytol from endogenous iron and localize it unequivocally in brain tissue. Intravenous injection of ferumoxytol into immune-competent rats that harbored human tumor xenograft-induced inflammatory brain lesions resulted in heterogeneous and lesion-specific signal enhancement on MRI scans *in vivo*. We used Dx1 immunolocalization and electron microscopy to identify ferumoxytol in affected tissue post-MRI. We found that ferumoxytol nanoparticles were taken up by astrocyte endfeet surrounding cerebral vessels, astrocyte processes, and CD163^{+}/CD68^{+} macrophages, but not by

Corresponding Author: Dr. Edward A. Neuwelt, Oregon Health & Science University, 3181 Sam Jackson Park Road, L603, Portland, OR 97239-3011, Contact Number: 503-494-5626, Fax Number: 503-494-5627, neuwelte@ohsu.edu.
(mcconneh@ohsu.edu)
(schwartd@ohsu.edu)
(brian@brianerichardson.com)
(woltjerr@ohsu.edu)
(muldoonl@ohsu.edu)

The authors declare that they have no competing interests in this study.

tumor cells. These results provide a biological basis for the delayed imaging changes seen with ferumoxytol and indicate that ferumoxytol-MRI can be used to assess the inflammatory component of brain lesions in the clinic.

Graphical Abstract

An ultrasmall superparamagnetic iron oxide nanoparticle (ferumoxytol) is used off-label as a contrast agent for magnetic resonance imaging of neuroinflammation in an immune-competent rat model. Dx1 (an anti-dextran monoclonal antibody) interacts with the modified carbohydrate coating of ferumoxytol, facilitating localization of the nanoparticles after extravasation from brain vasculature and phagocytosis by astrocytes and macrophages. The model is clinically relevant and recapitulated features of ferumoxytol localization in human glioblastoma multiform biopsy tissues.
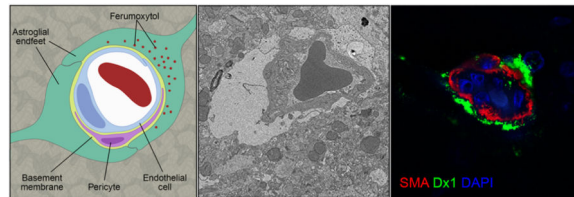
Keywords

Neuroinflammation; MRI; Iron oxide nanoparticles; macrophages; contrast agents

INTRODUCTION

Neuroinflammation is common in central nervous system (CNS) pathologies and causes changes in the cerebrovasculature and brain parenchyma that can be inconsistent and subtle, complicating detection of inflammatory processes with magnetic resonance imaging (MRI). Because neuroinflammation results in tissue changes that occur before loss of function, *in vivo* imaging of inflammation is of significant clinical interest. Such imaging is enabled by ferumoxytol, a viral-sized (17-31 nm) ultrasmall superparagmagnetic iron oxide (USPIO) nanoparticle [1, 2]. Ferumoxytol is approved by the Federal Drug Administration for treatment of iron deficiency anemia in patients with chronic kidney disease, but can be used off-label as a MRI contrast agent to detect CNS lesions and vascular abnormalities in brain [2-4]. While conventional gadolinium-based contrast agents allow rapid, transient, non-specific imaging of blood-brain barrier (BBB) permeability, they cannot differentiate neuroinflammation due to trauma from that due to tumor, for example [5]. The USPIO nanoparticle ferumoxytol is an emerging alternative approach for contrast enhancement in neuroimaging because, during neuroinflammation, it traffics from systemic circulation to reactive lesions and increases the contrast between affected and normal tissues [1]. Ongoing phase II clinical trials using ferumoxytol in patients with high-grade gliomas and multiple sclerosis plaques show that ferumoxytol-contrasted MRI may resolve phenomena including vascular changes, altered BBB permeability, long-term tissue changes in tumors, brain parenchyma, and neurological lesions on MRI (clinicaltrials.gov NCT00660543) [2, 6-8]. Despite these clinical advances, the timing and mechanisms of ferumoxytol trafficking into the brain, uptake into neuroinflammatory lesions, and cell-type specificity are unknown. The lack of information

on ferumoxytol localization is due in part to a lack of specific immunohistochemical markers. Perls' Prussian blue staining is the method typically used to assess the *ex vivo* tissue distribution of ferumoxytol along with electron microscopy methods [9, 10]. However, Perls' stain is an imperfect method to measure ferumoxytol localization because of its relatively low sensitivity and because it cannot reliably distinguish between the nanoparticle and endogenous (e.g. hemorrhage-derived) iron deposits. Here, we demonstrate that an anti-dextran monoclonal antibody (Dx1) reproducibly and specifically associates with the modified dextran coating of the ferumoxytol nanoparticle, allowing us to localize it in tissues *ex vivo* and differentiate ferumoxytol from endogenous iron.

We hypothesized that the enhanced BBB permeability resulting from acute neuroinflammation would allow targeted delivery of ferumoxytol nanoparticles to inflammatory lesions. To that end, we developed and characterized a model of localized inflammatory lesion using intracerebral injection of immunogenic human tumor cells in immune-competent rats. Our results show that ferumoxytol nanoparticles traffic from system circulation to reactive lesions during neuroinflammation, are taken up in a cell-specific manner, and can be detected over time using non-invasive MRI techniques. We present a novel correlate of neuroinflammation that can improve diagnostic imaging and response characterization across numerous neuropathologies.

METHODS

Cell Culture and Reagents

H460 non-small cell lung carcinoma cells were purchased from American Type Culture Collection (Manassas VA), used at a passage number below 20, and cultured in RPMI 1640 growth medium (Corning Life Sciences—Mediatech, Manassas VA USA) with 1% Penicillin/Streptomycin, 0.1% Gentamicin (Life Technologies, Eugene OR USA), and 10% FBS in 5% CO_2 at 37°C. U87 glioma cells were purchased from American Type Culture Collection (Manassas VA USA), used at a passage number below 20, and cultured in EMEM growth medium (Corning Life Sciences—Mediatech, Manassas VA USA) with 1% Penicillin/Streptomycin (Life Technologies, Eugene OR USA), 0.1% Gentamicin (Life Technologies, Eugene OR USA), and 10% FBS in 5% CO_2 at 37°C. Ferumoxytol (Feraheme®) was obtained from AMAG Pharmaceuticals Inc., Cambridge, MA USA.

Neuroinflammation Model

The care and use of animals was approved by the Institutional Animal Care and Use Committee and was supervised by the OHSU Department of Comparative Medicine. Adult female, immune-competent heterozygous nude rats (rnu/+) (200-300 g) were anesthetized with IP ketamine (60 mg/kg) and diazepam (7.5 mg/kg). To induce neuroinflammation, 10 μL of either H460 human non-small cell lung carcinoma cells (10^6 cells/μL, >90% viability) (n=6) or U87 glioma cells (n=3) were injected into the right caudate nucleus (Bregma= 0; lateral 0.31 cm; vertical - 0.65 cm) of each rat at a rate of 1 μL/min. To control for any inflammation due to the inoculation procedure, 10 μL of 0.9% NaCl was injected into the contralateral caudate nucleus (Bregma= 0; lateral −0.31 cm; vertical −0.65 cm) of each rat using a stereotactic frame.

Intravenous Ferumoxytol Administration

Rats were anesthetized with 2% mask isoflurane with oxygen. Ferumoxytol (30 mg/mL) (50 mg/kg body weight) was delivered over 60 seconds using a 24-gauge IV catheter in the lateral tail vein. For the pilot MRI study, ferumoxytol was administered at 0 (n=2), 24 (n=7), or 48 (n=2) hours after the inflammatory insult. Control animals instead received an equivalent volume of 0.9% NaCl IV (n=2).

Magnetic Resonance Imaging

MRI was performed 24 hours after ferumoxytol administration using a horizontal bore 11.75 T (Bruker Scientific Instruments, Billerica MA) under IP dexmedetomidine (0.6 mg/kg) (Zoetis, Lincoln NE) and ketamine (15 mg/kg) (sedation. T_1-weighted images were acquired with a fast low angle shot gradient-echo sequence (repetition time [TR]/echo time [TE]= 160.0 ms/1.6 ms, flip angle = 25°, 25 slices, inplane field of view (FOV) = 32×32 mm, matrix = 256×256, number of averages = 4, total acquisition time = 2.75 min). T_2-weighted images were acquired with a Rapid Acquisition and Refocused Echoes (RARE) spin-echo sequence (TR/TE = 4020.6 ms/11.8 ms, RARE factor = 8, 25 slices, FOV = 32×32 mm, matrix = 256×256, number of averages = 1, total acquisition time = 2.13 min). Images were processed using AFNI [11]. Briefly, images were compiled to NIFTI format, corrected for B_1 inhomogeneity using 3dUnifize, with manual thresholding and clustering performed to isolate the contrast-enhanced region-of-interest (ROI) on the T_1-weighted image. The ROI was then inverted along the midsagittal axis (3dLRflip) in order to extract image values in the NaCl-inoculated hemisphere (3dmaskave). The ROI was then superimposed on T_2-weighted images, and the same value-extraction process was performed. As the animals were fully anesthetized for the entire MRI session, no between-scan coregistration was necessary.

Immunohistochemistry

Immediately after MRI, rats were euthanized with a lethal dose of IV euthasol (Virbac, Fort Worth TX). Whole brains were removed for processing, fixed in 4% paraformaldehyde (Tousimis, Bethesda MD) at room temperature for 48 h and processed into paraffin blocks. Paraffin-embedded, 7-μm-thick tissue sections were cut from control and experimental rat brain hemispheres and mounted onto charged microscope slides. Immunohistochemical stains were applied to sections after deparaffinization and antigen retrieval (5 minutes at room temperature in 95% formic acid followed by 30 minutes incubation in citrate buffer, pH 6.0, at 80°C). Tissue sections were blocked with 3% nonfat dry milk in phosphate-buffered saline and stained with antibodies to the macrophage markers CD68 (AbCam, Cambridge MA, catalog #AB125212) (1:200) or CD163 (Biorad ABDSerotec Inc., Raleigh NC, catalog #MCA342R) (1:2500), the astrocyte marker glial fibrillary acidic protein (GFAP) (Sigma-Aldrich, St. Louis MO, catalog #G9269) (1:2500), or dextran (Dx1) (Stemcell Technologies, Vancouver Canada, catalog #60026) (1:100). Results were visualized after application of appropriate secondary antibodies using diaminobenzidine or Vector Red (Vector Laboratories, Burlingame, CA) as chromogens using an Olympus Bx50 microscope.

Immunofluorescent Histochemistry

Seven-μm-thick paraffin-embedded tissue sections of formalin-fixed control and experimental rat brain hemispheres were mounted onto charged microscope slides, deparaffinized, subjected to antigen retrieval as described above, blocked with 10% BSA, and simultaneously incubated with antibodies against Dx1 and either α-smooth muscle actin (SMA) (AbCam, Cambridge MA, catalog #AB5694) (1:2500) (a vascular smooth muscle cell marker) or CD68 (AbCam, Cambridge MA, catalog # AB125212) (1:200), all diluted in 1% BSA. Antibody labeling was visualized using Alexa-conjugated fluorescent secondary antibodies (1:500, Life Technologies, Grand Island, NY.) Sections were treated with Autofluorescence Eliminator Reagent (Millipore, Billerica, MA) and mounted using Prolong Gold antifade agent with DAPI (Life Technologies). Tissue was imaged using a Zeiss LSM 780 confocal microscope (Carl Zeiss, Oberkochen, Germany) at the OHSU Advanced Light Microscopy core facility. Post-acquisition processing was performed using ImageJ software (NIH, Bethesda MD).

Human subjects

Tissue collection analysis was performed at Oregon Health & Science University with informed consent by subjects and in accordance with the requirements of the local Institutional Review Board. For the histological review and immunohistochemical studies, the pathologic diagnoses of glioblastoma were established by a neuropathologist and reviewed (by RLW) to confirm the diagnosis and assess tumor vasculature. Immunohistochemical evaluation was performed on archival tissue from 2 subjects. Immunohistochemical staining was performed as described above.

Tissue sampling

For rat tissue, dextran immunostaining was consistently distributed throughout the macrophage-rich core of the lesion and a representative area was depicted in the figures. Human tumor tissue was derived from the MRI T1- enhancing portion of a glioblastoma and Dx1 immunostaining was present multifocally throughout the area of the tumor and was present most conspicuously around vessels supplying viable tumor.

Electron Microscopy

Tissues from the neuroinflamed and saline-inoculated caudate nuclei of rats (n=2) were collected 24 h after ferumoxytol administration and fixed in 1.5% glutaraldehyde, 1.5% paraformaldehyde in 0.1 mol/L sodium cacodylate buffer (pH 7.4). The tissue were then postfixed in buffered osmium tetroxide, stained *en bloc* with 1% uranyl acetate, dehydrated in graded ethanol solutions, and then embedded in epoxy resin. Sections of 60–90 nm thicknesses were placed onto 200 mesh grids, stained with uranyl acetate and lead citrate, then examined with a Techni 12 electron microscope (FEI, Hillsboro OR) at 80 Kv. Digital images were acquired using a 16 megapixel Advanced Microscopy Techniques camera (AMT, Woburn MA). Nanoparticle diameter was measured using the scope measurement tool, which is calibrated against a diffraction grating replica. Post-acquisition processing and additional nanoparticle diameter measurements (figure insets) were performed using ImageJ software.

RESULTS

Pilot characterization of the tumor xenograft neuroinflammation model

We performed a pilot study investigating magnetic resonance (MR) signal changes at intracerebral lesion sites in order to characterize the time course of inflammatory changes induced by tumor xenograft placement. We acquired T_1- and T_2-weighted MRI experiments at 11.75 T 24, 48, and 72 hours after insult. Ferumoxytol was administered 24 hours prior to each scanning session. We found that peak susceptibility and peak enhancement occurred 48 h post-insult on T_2-weighted and T_1-weighted images, respectively (Figure 1F). Therefore, the 48 h time point was used for all subsequent experiments (Figure 2). Ferumoxytol resulted in MR signal changes at all reactive inflammatory lesions. T_1-weighted sequences produced areas of hypointensity within the core of the lesion (due to T_2 contributions from areas of high contrast agent concentration) and a peripheral hyperintense ring around the lesion (Figure 1A). T_2-weighted experiments showed a marked focal signal loss at the insult site due to high concentrations of ferumoxytol (Figure 1D). Color maps depicting the values within each ROI for both T_1- and T_2-weighted images are shown in Figures 1B and 1E, respectively. Saline injection into the contralateral hemisphere did not result in MRI signal changes (Figure 1A, white arrowhead). The ratio of MRI values (lesion/saline) averaged over each ROI for 24, 48, and 72 h measurements were 1.23, 1.41, and 1.19 for T_1-weighted images and 0.72, 0.53, and 0.94 for T_2-weighted, respectively.

Ferumoxytol traffics from systemic circulation to reactive lesions

Because MRI signal enhancement occurred in xenografted but not saline-injected hemispheres (Figure 1A), we determined whether these signal changes were due to ferumoxytol extravasation and parenchymal infiltration in the affected hemisphere. Immunohistochemical analyses of the inflamed hemisphere containing the xenograft demonstrated CD68- and CD163-rich lesions with live tumor cells located peripherally (Figure 3B and 3C). We used a monoclonal anti-Dx1 antibody to detect the ferumoxytol nanoparticle coating and observed strong intracellular staining in areas that colocalized with the CD68^{+} and CD163^{+} cells at the lesion (Figure 3A). The contralateral (saline-injected) hemispheres were lesion-negative and showed no CD163 or Dx1 reactivity after IV ferumoxytol (data not shown). Rats that received IV saline after xenograft placement instead of IV ferumoxytol had similar CD163^{+}-rich lesions (Figure 3F) but showed no Dx1 reactivity (Figure 3E).

In addition to the intracellular Dx1 staining within the lesion, we observed Dx1 staining in cells outside the lesion that were macrophage-negative (Figure 3A arrowhead). Astrocytes are known to be capable phagocytes following activation; we analyzed CD163/CD68-negative, Dx1-positive regions for GFAP-reactivity and found robustly staining cells of astrocytic morphology (Figure 3D arrowhead).

Ferumoxytol uptake at inflammatory lesions is cell type-specific

We confirmed cell-specific uptake of ferumoxytol using double immunofluorescence labeling. Immunostaining for Dx1 and CD68 confirmed that ferumoxytol was intracellularly localized to CD68^{+} cells in the lesions (Figure 4A). In these cells we noted membrane-

localization of CD68 and diffuse, cytoplasmic Dx1 localization with distinct nuclear exclusion. Control rats that received saline instead of ferumoxytol showed similar CD68^{+} cells at the lesion but did not display Dx1 reactivity (Figure 4B). We next identified nearby vasculature as the source of ferumoxytol using multichannel high-resolution confocal microscopy. Within a z-stack of optical sections, dual staining for Dx1 and SMA revealed abundant perivascular ferumoxytol and sparse, residual ferumoxytol within the vascular lumen of precapillary arterioles (Figure 4C). The confinement of Dx1 staining around the vasculature suggested that some of the nanoparticles might become trapped within the basal lamina basement membrane of the neurovascular unit and be unable to extravasate, a phenomenon known to occur with iron nanoparticles that are >30 nm in diameter [12]. We repeated the dual staining for Dx1 and SMA on biopsy tissue from a human patient with glioblastoma who received IV ferumoxytol prior to MRI and gross tumor resection and observed the same perivascular delimitation of Dx1 staining around cerebral vessels (Figure 4D). To identify the cellular or subcellular perivascular structure in which ferumoxytol accumulates, we performed electron microscopy on tissue from inflamed and control rat brain hemispheres. Twenty-four h after administration, ferumoxytol nanoparticles were found in dilated astroglial endfeet-ensheathing capillaries (Figure 5A) and were identified as electron-dense particles ~30 nm in diameter (Figure 5A inset). Swollen astrocyte endfeet are an ultrastructural feature that has been noted previously in ischemic rodent brain [13]. Astroglial processes in the parenchyma also showed abundant ferumoxytol uptake (Figure 5B). Finally, we confirmed intracellular ferumoxytol localization within lysosome-rich CNS macrophages (Figure 5C). In agreement with our immunohistochemical findings that showed more robust Dx1 staining in macrophages than in areas of gliosis (Figure 4A, macrophages versus arrowhead), ferumoxytol nanoparticles were more abundant in macrophages and more aggregated in appearance (Figure 5C) than in astrocytic endfeet (Figure 5A) or processes (Figure 5B). The saline-inoculated hemispheres of rats that received IV ferumoxytol were ferumoxytol-negative and did not display swollen astrocytic endfeet (Figure 5D).

DISCUSSION

An important barrier to the use of ferumoxytol in the clinic is that the timing and pattern of delayed parenchymal MRI signal enhancement can be highly variable, which confounds meaningful interpretation of MRI data [14-16]. These inconsistencies led us to believe that the localization of the nanoparticles during and after their extravasation may underlie the variable timing and pattern of parenchymal MRI enhancement. In the current study, we evaluated ferumoxytol imaging characteristics and entry into the brain using a human tumor xenograft model of acute neuroinflammation in rat. We found that ferumoxytol USPIO nanoparticles extravasate from the cerebrovasculature and traffic to reactive CNS lesions within 24 h of their entry into the systemic circulation, but only if neuroinflammation is present. Our finding that ferumoxytol extravasation into the brain parenchyma only occurred in hemispheres containing inflammatory lesions indicates an inflammation-dependent increase in cerebrovascular permeability and supports the well-characterized role of the cerebrovascular BBB in bridging peripheral and central innate immune responses [17]. Our results demonstrated cell-specific uptake of ferumoxytol by astrocyte endfeet surrounding

cerebral vessels, astrocyte processes, and CD163$^+$/CD68$^+$ macrophages in the brain. In addition, we found that our model of neuroinflammation was clinically relevant, as it recapitulated features of ferumoxyol uptake and localization in the vasculature of GBM patients.

The mechanism by which ferumoxytol extravasates from cerebral vasculature remains unclear, but may involve 1) passive diffusion of free, non-cell associated nanoparticles across a disrupted BBB [18, 19] or 2) active transport across the BBB within infiltrating monocytes [19, 20]. Our electron microscopy data is most consistent with a mechanism involving free nanoparticle trafficking, as free nanoparticles were observed in astrocyte endfeet and processes that ensheath brain vascular endothelial cells and, as such, should be the first cells to encounter extravasating nanoparticles [19, 21]. Consistent with reports showing *in vitro* iron oxide nanoparticle uptake by astrocytes [22-24], we found ferumoxytol within swollen astrocytic endfeet 24 h after its administration. Interestingly, ferumoxytol was only present in endfeet that did not juxtapose endothelial cell nuclei, suggesting that the nanoparticles do not cross endothelial cell nuclei though such permeability has been reported previously for *in vitro* systems [25, 26]. Extravasation of nanoparticles across disrupted endothelial cell tight junctions is also plausible, but we were unable to resolve such structures in our images.

An alternative mechanism for ferumoxytol extravasation from the cerebrovasculature may involve Trojan horse-like transport across the BBB within infiltrating monocytes [20]. This mechanism was not supported by our histological or electron microscopy data, but only insofar as our tissue sections did not capture an extravasation event. Previous studies investigating the ability of USPIO (~20-30 nm particle diameter) and larger SPIO (~60-150 nm particle diameter) nanoparticles to label leukocytes *in vivo* for MRI cell tracking found that only larger SPIO nanoparticles were appreciably taken up by mononuclear leukocytes [27, 28]. Differential cellular uptake of USPIO nanoparticles can depend on many variables, including particle coating composition, particle charge, and particle size. In 2012, Thu *et. al.* demonstrated that effective *in vitro* labeling of mononuclear leukocytes with ferumoxytol could only occur in the absence of serum and only if the USPIO nanoparticle was first complexed with heparin and protamine (effectively increasing the size of the nanoparticle and strength of the stimulus for cell uptake) [10]. The rare systemic uptake of ferumoxytol reported and our histological and electron microscopy data both support a mechanism wherein ferumoxytol traffics into the CNS as a free nanoparticle. Importantly, our data does not rule out the possibility that, once inside the brain, free ferumoxytol is taken up by infiltrating blood monocytes that differentiate into macrophages upon CNS entry. Indeed, the vast numbers of CD163+/CD68+ macrophages observed at the reactive lesion sites suggest such a scenario.

Our histological identification of ferumoxytol nanoparticles in tissue via Dx1 immunohistochemistry provides new insight into disease pathogenesis in affected tissues. The opposing ring enhancement patterns found on T_1 and T_2-weighted MRI reflect our immunohistochemistry findings that clearly show ferumoxytol uptake in densely packed macrophages in the core of the lesion and reactive astrocytes around the margin of the lesion but not in viable tumor cells. The non-invasive, *in vivo* identification of immune reactivity to

inflammatory CNS insult at sub-millimeter resolution using ferumoxytol-MRI may provide a more expansive view of affected tissue and provide more accurate targets for invasive biopsy in CNS lesions than current standard of care contrast-enhanced MRI. The nonlinearity of T_1-weighted contrast with respect to ferumoxytol concentration provides further specificity of microenvironmental heterogeneity in and around a lesion. Strong T_1-weighted signal dropout in regions of intense Dx1 staining within macrophages suggests a T_2 shortening contribution to T_1-weighted images in regions with very high ferumoxytol concentration. We observed T_1 hyperintensity among areas of diffuse Dx1 staining on the lesion periphery that suggested lower ferumoxytol concentrations, possibly due to nanoparticles localized within the processes or endfeet of reactive astrocytes. These findings suggest that ferumoxytol-MRI may be able to differentiate immunological microenvironments in the brain.

Limitations of our study include a relatively high dose of administered ferumoxytol (compared to human dosages; although, as seen in Figure 4D, we were able to detect ferumoxytol in human tissue) and an experimental model that relies on the acute inflammatory effects of a xenograft in rat that may not accurately replicate what occurs over time in human metastatic or primary CNS tumors. Furthermore, we used immune-competent rats in this study, but patients with brain tumors often display a degree of immunologic anergy; our use of a fully immune-competent animal may not adequately recapitulate the state of these patients. Future work will investigate the validity of our findings using hematogenous metastasis or spontaneous glioblastoma models of inflammation.

In conclusion, our study is the first confirmation that ferumoxytol nanoparticles are taken up by astrocyte endfeet surrounding cerebral vessels, astrocyte processes, and CD163^{+}/CD68^{+} macrophages in a model of a brain inflammatory lesion. We identify a novel and specific marker of the ferumoxytol carboxymethyldextran coating, Dx1, which allows ferumoxytol to be unambiguously identified in tissue and differentiated from endogenous iron. We present a clinically relevant animal model of acute neuroinflammation with which to study ferumoxytol nanoparticle extravasation that recapitulates features of ferumoxyol localization in the vasculature of GBM patients. Moreover, we demonstrate that areas of Dx1 reactivity in CNS tissue match well with areas of signal change on MR images. Future investigations will quantify and correlate immune-based USPIO nanoparticle uptake and CNS infiltration with USPIO-induced MR signal alterations, which we believe will assist interpretation of MR images in the clinical setting, guide CNS biopsy, and provide unique information to facilitate diagnostic specificity.

Acknowledgements

ABBREVIATIONS

CNS	central nervous system
MRI	magnetic resonance imaging
USPIO	ultrasmall superparamagnetic iron oxide
BBB	blood-brain barrier

References

1. Weinstein J, Varallyay CG, Dosa E, Gharmanov S, Hamilton B, Rooney WD, et al. Superparamagnetic iron oxide nanoparticles: Diagnostic magnetic resonance imaging and potential therapeutic applications in neurooncology and CNS inflammatory pathologies, a review. J Cereb Blood Flow Metab. 2010; 30:15–35. [PubMed: 19756021]

2. Iv M, Telischak N, Feng D, Holdsworth SJ, Yeom KW, Daldrup-Link HE. Clinical applications of iron oxide nanoparticles for magnetic resonance imaging of brain tumors. Nanomedicine (Lond). 2015; 10:993–1018. [PubMed: 25867862]

3. Dósa E, Tuladhar S, Muldoon LL, Hamilton BE, Rooney WD, Neuwelt EA. MRI using ferumoxytol improves the visualization of central nervous system vascular malformations. Stroke. 2011; 42:1581–1588. [PubMed: 21493906]

4. Lu M, Cohen MH, Rieves D, Pazdur R. FDA report: Ferumoxytol for intravenous iron therapy in adult patients with chronic kidney disease. Am J Hematol. 2010; 85:315–319. [PubMed: 20201089]

5. Enochs WS, Ackerman RH, Kaufman JA, Candia M. Gadolinium-enhanced MR angiography of the carotid arteries. J Neuroimaging. 1998; 8:185–190. [PubMed: 9780848]

6. Farrell BT, Hamilton BE, Dosa E, Rimely E, Nasseri M, Gahramanov S, et al. Using iron oxide nanoparticles to diagnose CNS inflammatory diseases and PCNSL. Neurology. 2013; 81:256–263. [PubMed: 23771486]

7. Gahramanov S, Muldoon LL, Varallyay CG, Li X, Kraemer DF, Fu R, et al. Pseudoprogression of glioblastoma after chemo- and radiation therapy: diagnosis by using dynamic susceptibility-weighted contrast-enhanced perfusion MR imaging with ferumoxytol versus gadoteridol and correlation with survival. Radiology. 2013; 266:842–852. [PubMed: 23204544]

8. Nasseri M, Gahramanov S, Netto JP, Fu R, Muldoon LL, Varallyay C, et al. Evaluation of pseudoprogression in patients with glioblastoma multiforme using dynamic magnetic resonance imaging with ferumoxytol calls RANO criteria into question. Neuro Oncol. 2014; 16:1146–1154. [PubMed: 24523362]

9. Khurana A, Nejadnik H, Chapelin F, Lenkov O, Gawande R, Lee S, et al. Ferumoxytol: a new, clinically applicable label for stem-cell tracking in arthritic joints with MRI. Nanomedicine (Lond). 2013; 8:1969–1983. [PubMed: 23534832]

10. Thu MS, Bryant LH, Coppola T, Jordan EK, Budde MD, Lewis BK, et al. Self-assembling nanocomplexes by combining ferumoxytol, heparin and protamine for cell tracking by magnetic resonance imaging. Nat Med. 2012; 26:463–467. [PubMed: 22366951]

11. Cox RW. AFNI: software for analysis and visualization of functional magnetic resonance neuroimages. Comput Biomed Res. 1996; 29:162–173. [PubMed: 8812068]

12. Muldoon LL, Pagel MA, Kroll RA, Roman-Goldstein S, Jones RS, Neuwelt EA. A physiological barrier distal to the anatomic blood-brain barrier in a model of transvascular delivery. AJNR Am J Neuroradiol. 1999; 20:217–222. [PubMed: 10094341]

13. Lukaszevicz AC, Sampaio N, Guegan C, Benchoua A, Couriaud C, Chevalier E, et al. High sensitivity of protoplasmic cortical astroglia to focal ischemia. J Cereb Blood Flow Metab. 2002; 22:289–298. [PubMed: 11891434]

14. Dósa E, Guillaume DJ, Haluska M, Lacy CA, Hamilton B, Njus JM, et al. Magnetic resonance imaging of intracranial tumors: intra-patient comparison of gadoteridol and ferumoxytol. Neuro Oncol. 2011; 13:251–260. [PubMed: 21163809]

15. Hamilton BE, Nesbit GM, Dosa E, Gahramanov S, Rooney B, Nesbit EG, et al. Comparative analysis of ferumoxytol and gadoteridol enhancement using T1- and T2-weighted MRI in neuroimaging. AJR Am J Roentgenol. 2011; 197:981–988. [PubMed: 21940589]

16. Muldoon LL, Manninger S, Pinkston KE, Neuwelt EA. Imaging, distribution, and toxicity of superparamagnetic iron oxide magnetic resonance nanoparticles in the rat brain and intracerebral tumor. Neurosurgery. 2005; 57:785–796. [PubMed: 16239893]

17. Engelhardt B. Immune cell entry into the central nervous system: involvement of adhesion molecules and chemokines. J Neurol Sci. 2008; 274:23–26. [PubMed: 18573502]

18. Neuwelt EA, Hamilton BE, Varallyay CG, Rooney WR, Edelman RD, Jacobs PM, et al. Ultrasmall superparamagnetic iron oxides (USPIOs): a future alternative magnetic resonance (MR) contrast agent for patients at risk for nephrogenic systemic fibrosis (NSF)? Kidney International. 2009; 75:465–474. [PubMed: 18843256]

19. Petters C, Irrsack E, Koch M, Dringen R. Uptake and metabolism of iron oxide nanoparticles in brain cells. Neurochem Res. 2014; 39:1648–1660. [PubMed: 25011394]

20. Brochet B, Deloire MS, Touil T, Anne O, Caille JM, Dousset V, et al. Early macrophage MRI of inflammatory lesions predicts lesion severity and disease development in relapsing EAE. Neuroimage. 2006; 32:266–274. [PubMed: 16650776]

21. Virgintino D, Monaghan P, Robertson D, Errede M, Bertossi M, Ambrosi G, et al. An immunohistochemical and morphometric study on astrocytes and microvasculature in the human cerebral cortex. Histochem J. 1997; 29:655–660. [PubMed: 9413738]

22. Hohnholt MC, Geppert M, Luther EM, Petters C, Bulcke F, Dringen R. Handling of iron oxide and silver nanoparticles by astrocytes. Neurochem Res. 2013; 38:227–239. [PubMed: 23224777]

23. Geppert M, Hohnholt MC, Thiel K, Nurnberger S, Grunwald I, Rezwan K, et al. Uptake of dimercaptosuccinate-coated magnetic iron oxide nanoparticles by cultured brain astrocytes. Nanotechnology. 2011; 22:145101. [PubMed: 21346306]

24. Jenkins SI, Pickard MR, Furness DN, Yiu HH, Chari DM. Differences in magnetic particle uptake by CNS neuroglial subclasses: implications for neural tissue engineering. Nanomedicine (Lond). 2013; 8:951–968. [PubMed: 23173710]

25. Hoff D, Sheikh L, Bhattacharya S, Nayar S, Webster TJ. Comparison study of ferrofluid and powder iron oxide nanoparticle permeability across the blood-brain barrier. Int J Nanomedicine. 2013; 8:703–710. [PubMed: 23426527]

26. Thomsen LB, Linemann T, Pondman KM, Lichota J, Kim KS, Pieters RJ, et al. Uptake and transport of superparamagnetic iron oxide nanoparticles through human brain capillary endothelial cells. ACS Chem Neurosci. 2013; 4:1352–1360. [PubMed: 23919894]

27. Wu YJ, Muldoon LL, Varallyay C, Markwardt S, Jones RE, Neuwelt EA. In vivo leukocyte labeling and characterization with intravenous ferumoxides/protamine sulfate for cellular magnetic resonance imaging. Am J Physiol – Cell Physiol. 2007; 293:C1698–1708. [PubMed: 17898131]

28. Oude Engberink RD, van der Pol SM, Dopp EA, de Vries HE, Blezer EL. Comparison of SPIO and USPIO for in vitro labeling of human monocytes: MR detection and cell function. Radiology. 2007; 243:467–474. [PubMed: 17456871]
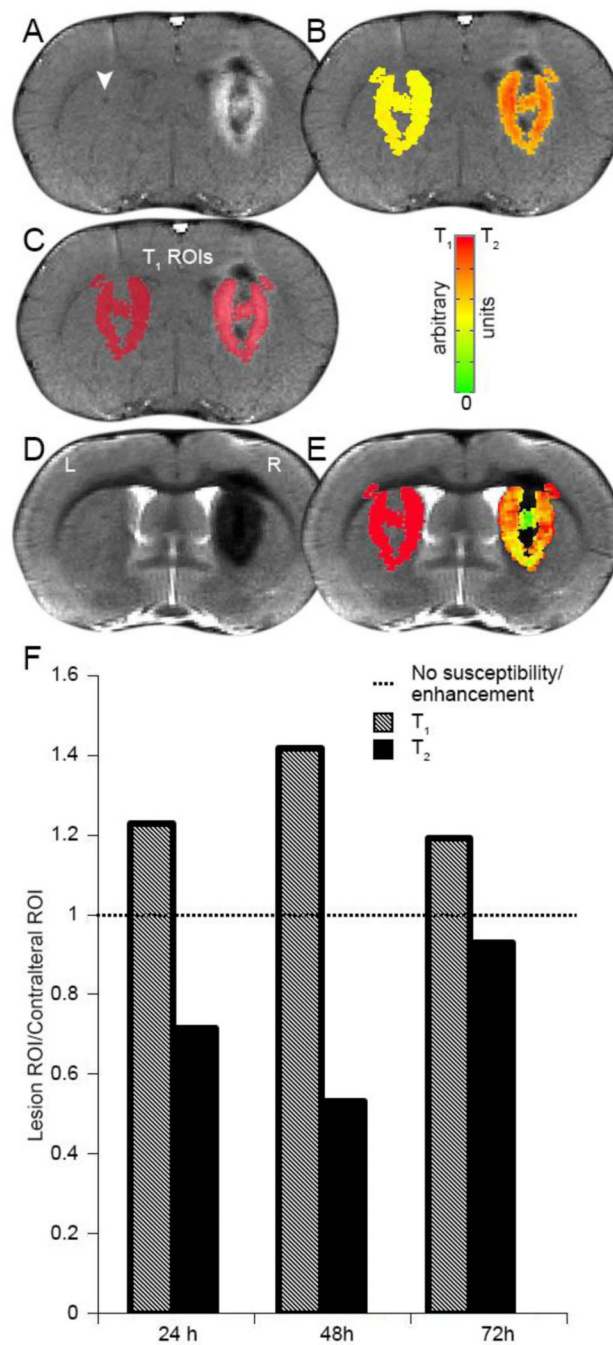
Figure 1. Maximum ferumoxytol MRI susceptibility/enhancement occurs 48 h post inflammatory insult

(**A, D**) T_1 and T_2-weighted MR images showing tumor cell and saline inoculation sites (right and left hemispheres, respectively) 48 h post-inoculation and 24 h post-ferumoxytol. (**B, E**) T_1 and T_2 intensity values displayed as a color map in arbitrary units within the region of interest (ROI). (**C**) ROI masks superimposed on the T_1-weighted image. (**F**) Voxel values within the lesion and contralateral ROIs were averaged over all voxels and compared graphically as a ratio for both T_1 (shaded)- and T_2 (black)-weighted MR images at each post-inoculation time point.
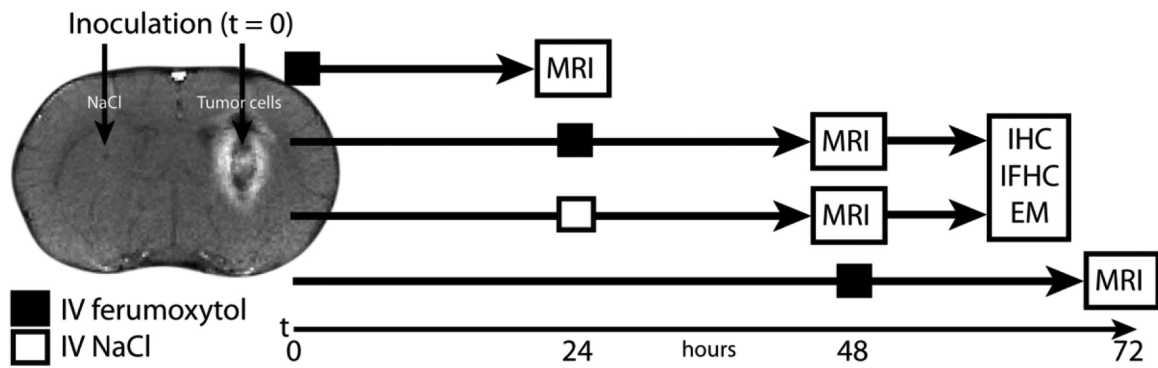
Figure 2. Experimental protocol schematic

For all experiments after the pilot MRI study, neuroinflammatory insult was administered at time (t)=0, IV ferumoxytol or saline (control) was administered at t=24 h, and MRI was performed at t=48 h. Immediately after MRI brains were extracted for immunohistochemistry (IHC) analysis, immunofluorescent histochemistry (IFHC) analysis, and electron microscopy (EM) analysis.
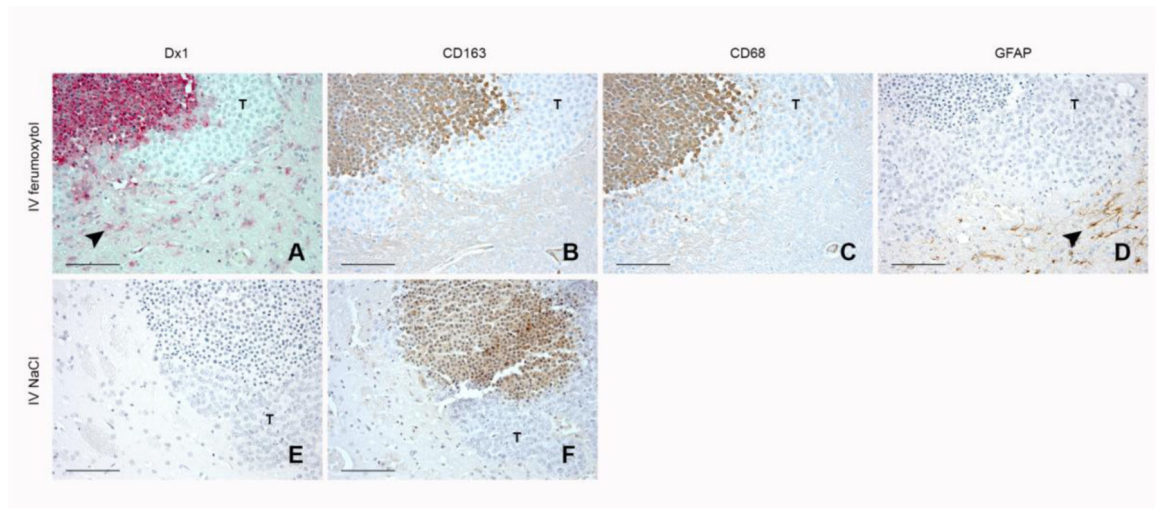
Figure 3. Immunostaining demonstrates that ferumoxytol traffics from the systemic circulation to reactive CNS lesions
(A-D) Immunostains performed 48 h after H460 cell inoculation into caudate nucleus and 24 h after IV ferumoxytol administration. A representative inflammatory lesion was immunostained with (A) Dx1 for the ferumoxytol coating (red), (B) CD163 for macrophages (brown), (C) CD68 for macrophages (brown), and (D) GFAP for astrocytes (brown). (E-F) Immunostains performed 48 h after H460 cell inoculation into caudate nucleus and 24 h after IV saline administration. A representative inflammatory lesion was immunostained with (E) Dx1 (red), and (F) CD163 (brown). All cell nuclei were counterstained with hematoxylin. **T** depicts live tumor cells (A-F). Arrowhead depicts reactive cells located outside of the main lesion (A-D). Scale bars, 100 μm.
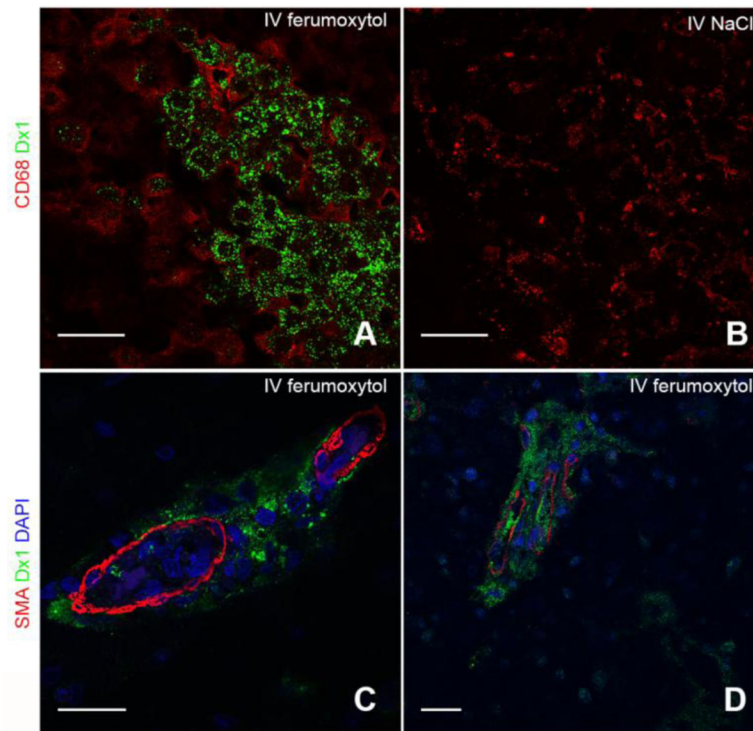
Figure 4. Immunofluorescence analysis reveals ferumoxytol localization within lesional macrophages and perivascular spaces

(A) Immunofluorescent image of CD68$^+$ (red) and Dx1$^+$ (green) macrophages in a representative inflammatory CNS lesion 48 h after H460 cell inoculation into caudate nucleus and 24 h after IV ferumoxytol administration. (B) Immunofluorescent image of CD68$^+$ and Dx1$^-$ macrophages in a representative inflammatory CNS lesion 48 h after H460 cell inoculation into caudate nucleus and 24 h after IV saline administration. Scale bars, 25 μm. (C) Representative immunofluorescent image demonstrating smooth muscle actin (SMA) (red) reactivity in the vascular wall and Dx1 (green) reactivity around a vessel near an inflammatory lesion. Scale bars, 25 μm. (D) Representative immunofluorescent image of human glioblastoma biopsy tissue demonstrating smooth muscle actin (SMA) (red) reactivity in the vascular wall and Dx1 (green) reactivity around cerebral vessels.
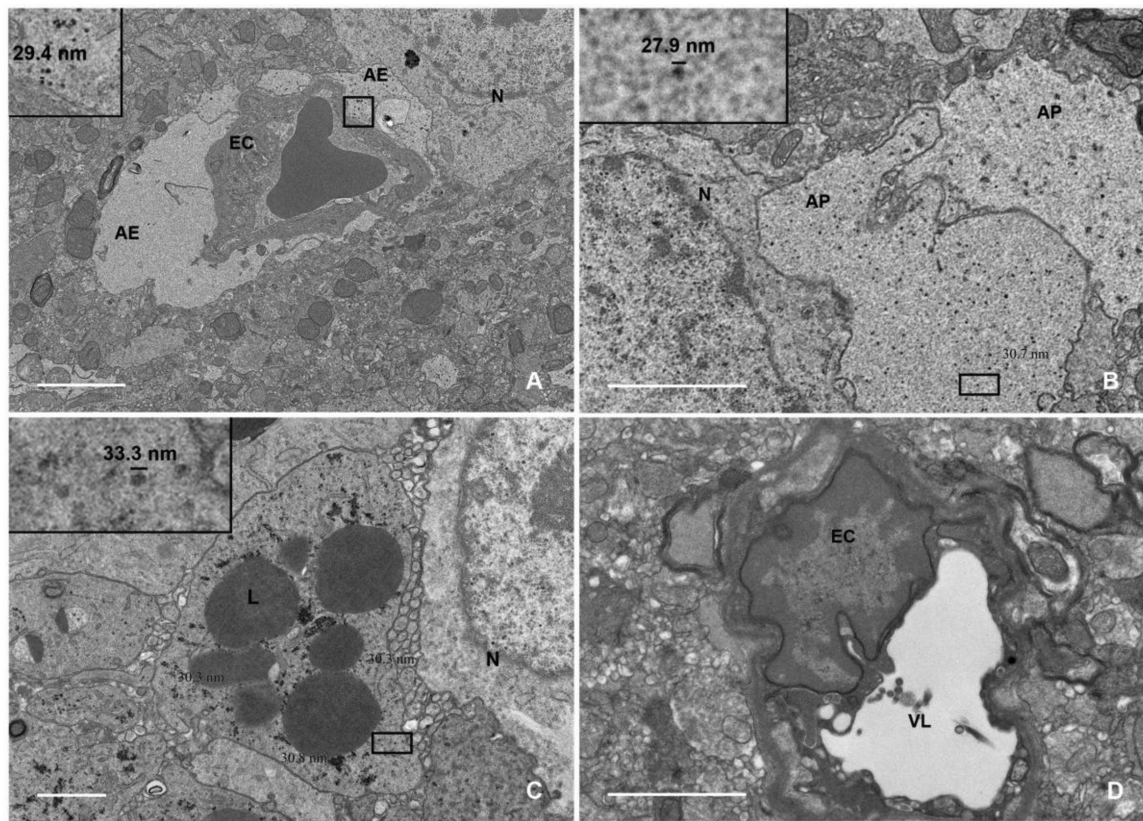
Figure 5. Ultrastructural analyses of CNS tissue show ferumoxytol localization within astrocyte endfeet, astrocyte processes, and phagocytic CNS macrophages

(A-C) Representative electron micrographs showing tissue from the caudate nucleus of neuroinflamed rats 24 h after IV ferumoxytol. **(A)** Capillary cross-section showing a single lumenal red blood cell and dispersed electron-dense ferumoxytol nanoparticles (inset) within the astrocyte endfoot not abutting the endothelial cell nucleus. The astrocyte endfoot abutting the vascular endothelial cell nucleus is swollen and void of ferumoxytol (magnification ×2900). Scale bar, 2 μm. **(B)** Two astrocyte processes showing dispersed, electron-dense ferumoxytol nanoparticles (inset) (magnification ×6800). Scale bar, 1 μm. **(C)** Activated CNS macrophage with lysosome-rich cytoplasm and abundant intracellular ferumoxytol nanoparticle accumulation (inset) (magnification ×6800). Scale bar 1 μm. **(D)** Electron micrographs showing tissue from the contralateral (saline-inoculated) caudate nucleus of neuroinflamed rats 24 h after IV ferumoxytol. Representative cerebral vessel cross-section showing no astrocyte endfoot swelling and no ferumoxytol uptake (magnification ×6800). Scale bar, 1 μm. N, neuron; EC, endothelial cell; AE, astrocyte endfoot; AP, astrocyte process; L, lysosome; VL, vessel lumen